JAAS

Accepted Manuscript

This is an *Accepted Manuscript*, which has been through the Royal Society of Chemistry peer review process and has been accepted for publication.

Accepted Manuscripts are published online shortly after acceptance, before technical editing, formatting and proof reading. Using this free service, authors can make their results available to the community, in citable form, before we publish the edited article. We will replace this *Accepted Manuscript* with the edited and formatted *Advance Article* as soon as it is available.

You can find more information about *Accepted Manuscripts* in the Information for Authors.

Please note that technical editing may introduce minor changes to the text and/or graphics, which may alter content. The journal's standard Terms & Conditions and the Ethical guidelines still apply. In no event shall the Royal Society of Chemistry be held responsible for any errors or omissions in this *Accepted Manuscript* or any consequences arising from the use of any information it contains.

ROYAL SOCIETY OF CHEMISTRY

www.rsc.org/jaas

Colour degradation of artworks: an *ab-initio* approach to X-ray, electronic and optical spectroscopy analyses of vermilion photodarkening

C. Hogan* F. Da Pieve†

November 7, 2014

Abstract

Light-induced photodarkening of the pigment vermilion (α-HgS, cinnabar), observed in historical museum paintings and in murals at archaelogical sites worldwide, is an intriguing phenomenon that has triggered intense study using microscopy and spectroscopy techniques. However, the origins of the degradation and the nature of the concomitant physical, chemical and structural transformations are not yet completely clear. We present a first-principles study based on state-of-the-art electronic structure methods which sheds light on this darkening phenomenon. The presence of secondary compounds proposed to form during the transformation of vermilion ($Hg_3S_2Cl_2$ polymorphs, Hg_2Cl_2, and $HgCl_2$) is confirmed using X-ray spectroscopy simulations, and their structural, electronic, and optical properties are analysed using different levels of theory and compared with

*Consiglio Nazionale delle Ricerche, Istituto di Struttura della Materia (CNR–ISM), via Fosso del Cavaliere 100, 00133 Rome, Italy; Department of Physics and European Theoretical Spectroscopy Facility (ETSF), Università di Roma "Tor Vergata", Via della Ricerca Scientifica 1, 00133 Rome, Italy, E-mail: conor.hogan@ism.cnr.it

†Laboratoire des Solides Irradiés, UMR 7642, CNRS-CEA/DSM, École Polytechnique, F-91128 Palaiseau, France and European Theoretical Spectroscopy Facility (ETSF), E-mail: fabiana.dapieve@gmail.com

experimental observations. A scheme for growth of α-$Hg_3S_2Cl_2$ on α-HgS is proposed, and possible formation and decomposition paths for the mercury chlorides are discussed. Approximations used in computing band gaps and band edges are examined in detail. This work highlights the key role that first-principles methods can play in the application of materials science to art conservation.

1 INTRODUCTION

Discolouration, degradation and colour-change phenomena of paintworks is a complex subject.[1–3] Their underlying causes are not always easily identified by scientists and conservators, as they range from factors such as dirt deposition and mold growths to the simultaneous action of light, heat, atmospheric conditions and contaminated air. Chemical and/or physical changes in the original pigments can thereby be activated and eventually play a role in their transformation. For example, certain pigments such as chrome yellow and Prussian blue are strongly discoloured by alkalis,[3] while Ultramarine decomposes under exposure to acidic fumes.[4] Formal quantitative studies are clearly necessary to shed light on these various factors. Nonetheless, there has up to now been little direct impact from microscopic simulations of these complicated processes.[5–8]

Colour degradation of paintworks induced by the action of light has recently attracted the attention of several scientific groups working with spectroscopy or microscopy techniques.[9–14] A well-known case is that of light-induced darkening of vermilion, as observed in mural paintings at archaeological sites and in paintings conserved in museums. Over the centuries, this red mercury(II) sulfide α-HgS with the cinnabar structure has been used as a red pigment in paintings. Its use has a lengthy history that spans several continents and eras, from prehistory in China and India to the Roman empire, from the Peruvian Chavin Empire in 500 BC to the medieval and Renaissance period. Archeological sites, cathedral wall paintings, and several famous masterpieces from major painters (including Rubens and the Italian masters), conserved in galleries and museums, are affected by its irreversible degradation. Cinnabar

is known to be photosensitive in the presence of halogen pollutants and to darken under illumination,[15–17] leading to an unwanted colour degradation. It is imperative to understand its origin in order to plan better conservation strategies.

The darkening was attributed by some authors[14,18–20] to a phase change to the black zincblende phase, β-HgS (metacinnabar). However, the detection of different chemical species in degraded samples through X-ray absorption near edge spectroscopy (XANES), Raman, and microscopy has prompted a closer examination of the phenomenon.[10–14,20,21] Halogens have been found to play a dominant role in the darkening process of photosensitive coatings that develop on α-HgS.[15–17] Spring *et al.*[20] inferred that vermilion is first transformed into the photosensitive α-$Hg_3S_2Cl_2$ (corderoite) after exposure to humidity and chloride ions. This α-$Hg_3S_2Cl_2$ was proposed to subsequently degrade into black β-HgS, white Hg_2Cl_2 (calomel) and elemental sulfur by a light-induced reaction. Using Raman microscopy, Spring *et al.* clearly identified Hg_2Cl_2 within white particles in the gray crust appearing on the surface of several paintings from the 15th century. Hg_2Cl_2 had previously been identified through X-ray diffraction studies[22] in the gray photodegradation product of α-$Hg_3S_2Cl_2$. Cotte *et al.* performed microscopic X-ray fluorescence (XRF) and X-ray absorption near edge spectroscopy (XANES) on samples of Pompeian paintings[10] and paintings from the Monastery of Pedralbes, Barcelona[11] and demonstrated the presence of chlorine and (light-coloured) sulfates on the surface of degraded HgS-samples,[10] as well as a mixture of HgS, Hg_2Cl_2 and α-$Hg_3S_2Cl_2$.[11] Keune *et al.*[13] performed scanning electron microscopy in combination with energy dispersive X-ray analysis on indoor paintings and observed that a black product is formed first, followed by a white compound. They proved that β-HgS cannot be produced and they identified for the first time another white reaction product (kenhsuite, γ-$Hg_3S_2Cl_2$). Another extended study combining elemental laboratory analysis with XRF and XANES measurements[12] on paint samples of different origin (*The Adoration of the Magi* by P.P. Rubens and wall paintings from the Monastery of Pedralbes) revealed the presence of Hg_2Cl_2, α-$Hg_3S_2Cl_2$ and γ-$Hg_3S_2Cl_2$. The analysis clearly revealed that photoactivation of the materials by UV irradiation is required to provoke the colour change and that chlorine is involved in the

degradation process. When non-degraded samples were illuminated by UV light,[10,12] a grey/black compound was observed, accompanied by white streaks having a higher relative amount of Cl, similar to the observations by Keune *et al.*[13] As also suggested by Cormack *et al.*,[23] the authors proposed that both Hg_2Cl_2 and α-$Hg_3S_2Cl_2$ are either formed simultaneously as degradation products of α-HgS, or that very soon after its formation α-$Hg_3S_2Cl_2$ degrades further to Hg_2Cl_2. No indications were found of the presence of $HgCl_2$, identified by Keune *et al.*[13] as a major degradation product, nor of black β-HgS. Fourier Transform Infra-Red spectroscopy (FTIR) has been applied to the analysis of vermilion-containing artworks,[24,25] and can differentiate α-HgS from β-HgS thanks to structures around 400 cm^{-1} appearing in the β-HgS spectrum.[26] However, no valuable information relevant to understanding cinnabar degradation has been obtained with FTIR. In a recent work,[27] we used state-of-the-art calculations to demonstrate that precipitation of elemental Hg at the α-HgS/α-$Hg_3S_2Cl_2$ surface can be induced by light in humid environments, a finding supported by subsequent electrochemical measurements on degraded α-HgS.[28] The presence of metallic Hg was thus proposed to be ultimately responsible for the darkening. A surficial layer of colloidal mercury on α-HgS was proposed as far back as 1938 by Dreyer as being responsible for the observed darkening.[29] In summary, therefore, various routes for degradation of red α-HgS have been proposed, but the exact mechanism and a possible solution for preventing degradation remain open questions.

Understanding such colour-changing phenomena constitutes a fascinating challenge, drawing from aspects of crystallography, surface chemistry and optical excitations. As quantum mechanics lies at the heart of these separate disciplines, it is clear that a comprehensive understanding of α-HgS photodarkening may be achieved through advanced first principles calculations. *Ab-initio* density functional theory (DFT) based on the Kohn-Sham (KS) theory of electronic structure is an invaluable tool for the understanding of ground state properties of systems in materials science, chemistry and biology. In order to explain a system's response to light, or to predict spectroscopic results, higher level theoretical approaches such as time dependent density functional theory (TDDFT) or many body perturbation theory (MBPT) are often needed. Such

approaches are indeed able to better describe the exchange and correlation interactions among electrons. Both TDDFT and MBPT are able to describe neutral excitations, i.e., electron-hole pair creation induced by optical absorption. MBPT also gives access to charged excitations, such as those probed by photoemission. Within MBPT, single particle excitations are generally described in terms of quasiparticles (electrons or holes *plus* their self energy). The so-called *GW* approximation is the state-of-the-art approach for computing quasiparticle energy levels, and has yielded excellent predictions of band levels and gaps for a wide class of materials.[30]

In this work, we expand upon the results obtained in our previous study.[27] We begin by introducing the main mercury compounds under study and provide a brief overview of the *ab-initio* methodologies used. We then clarify the main mineral composition of degraded painting samples through X-ray analyses of the pigments at K edges (which mainly reflects structural properties). This leads us to discuss in detail a possible mechanism of structural transformation of the original red pigment. Degradation of secondary minerals is subsequently discussed in terms of structural properties and orbital symmetries (α-$Hg_3S_2Cl_2$) and in terms of possible (photo)chemical processes in the two chloride phases, Hg_2Cl_2 and $HgCl_2$, the latter not always detected in experiments. This work demonstrates that a variety of properties affect the transformation, including the band gaps for photon absorption of the various compounds, the band edge positions, and the stability of the different subsequent observed compounds.

2 METHODOLOGY

2.1 Crystalline Hg compounds

Mercury compounds are intriguing materials that show unique structural, chemical and optical properties. In this work we consider several compounds that Hg forms with S and Cl. Mercury exhibits different oxidation states and is capable of forming complex and multiple associations. Cinnabar (α-HgS, space group $P3_221$, trigonal) is the form in which mercury is most commonly found in nature. Corderoite (α-$Hg_3S_2Cl_2$) is the most stable crystalline form of $Hg_3S_2Cl_2$ and has an isometric (cubic) structure with

space group $I2_13$. β-$Hg_3S_2Cl_2$ has space group $Pm3n$, while kenhsuite (γ-$Hg_3S_2Cl_2$) has an orthorhombic structure and is considered to be the second metastable polymorph of α-$Hg_3S_2Cl_2$.[31] Calomel (Hg_2Cl_2, space group I_4mmm) is a van der Waals crystal consisting of linear Cl-Hg-Hg-Cl molecules. It crystallizes in a tetragonal structure (D_{4h}^{17}) where the molecular axes are aligned along the tetragonal c axis. It is uncoloured and photosensitive. Last, mercuric chloride ($HgCl_2$) is constituted by linear triatomic molecular units, and is highly water soluble. Lattice parameters have been taken from the American Mineralogy database.

2.2 *Ab-initio* calculations

Calculations were performed within frameworks based upon density functional theory (DFT) in the generalized gradient approximation (GGA) using the functional parametrization of Perdew-Burke-Ernzerhof.[32] We used various computational tools designed for solid state systems, thus having periodic boundary conditions (in 1, 2, or 3 dimensions) and basis sets constructed of plane waves. Brillouin zone (BZ) integrations were carried out using dense k-point grids in order to ensure highly converged results to about 2 meV per formula unit: 6×6×4, 4×4×4, 6×6×4, 4×4×6, 4×4×6 for α-HgS, α-$Hg_3S_2Cl_2$, Hg_2Cl_2, γ-$Hg_3S_2Cl_2$, and $HgCl_2$, respectively.

X-ray response properties of bulk materials were calculated at the DFT level using the all electron (AE) code Wien2k.[33] Muffin-tin sphere radii R_{MT} were set as 2.45 Bohr for Hg and 1.9 Bohr for S and Cl, respectively, and $R_{MT}k_{max}$ is set to 8.0. XANES spectra were obtained in the full core hole approximation, i.e. introducing a frozen hole in the excited orbital and smearing the charge uniformly in space, on 2×2×2 supercells. A DFT approach is quite appropriate here as the systems under study are not strongly correlated and because we are exciting at the K edge (and hence excite only to the delocalized p states, generally well described by band theory). The good performance of the single particle picture offered by DFT within the final state rule with respect to more advanced theories has been discussed.[34]

Electronic structures (energy levels and band gaps) at the quasiparticle level were computed for bulk materials using many body perturbation theory (MBPT) as imple-

mented in the planewave and pseudopotential (PSP) code ABINIT.[35] In short, quasiparticle levels were obtained using the so-called *GW* approximation (*G*= Green's function, *W*= screened Coulomb interaction) for the electron and hole self energies, in the first perturbative step (G_0W_0, or 'one-shot *GW*'). A brief overview of the *GW* approach is given in the Appendix, along with a more detailed analysis of an important technical aspect, namely, the use of an appropriate plasmon-pole model of the dielectric response. Optical absorption spectra including excitonic effects were computed for α-HgS by solving the Bethe-Salpeter equation (BSE) with ABINIT. This calculation was performed on a shifted $12\times12\times10$ grid, including local field effects, and using the Tamm-Dancoff approximation, a scissor operator (obtained from the G_0W_0 result) and the iterative Haydock technique. The cutoff energy was set to 60 Ha, and all pseudopotentials used were norm-conserving.

The planewave/PSP code quantum-ESPRESSO[36] was used for DFT calculations of surface and interface structures. Cutoff parameters, pseudopotentials, and *k*-point meshes were chosen to be consistent with the bulk crystal calculations from ABINIT. Where known, unreconstructed cleavage planes were adopted: these correspond to $\{10\bar{1}0\}$ on α-HgS and $\{110\}$ on Hg_2Cl_2; otherwise, simple (1×1) electroneutral surfaces were chosen, i.e., (110) for α-$Hg_3S_2Cl_2$ and (100) for $HgCl_2$.[37] The surfaces were modeled within a supercell framework of repeated thick slabs separated by vacuum layers. This allowed us to determine the *absolute values* of the band edges for each system within DFT.

Finally, we corrected these band edges within an approximate *GW* approach, as full *GW* calculations are prohibitively heavy for these complex surfaces. A theorem by Perdew and Levy,[38] that extends Janak's theorem for calculating the work function[39] to non-metallic systems, states that although DFT can only provide a lower limit to the absolute value of the valence band maximum VBM (even in the case of an exact functional), it is formally exact for calculating the band gap center E_{BGC}. We thus combine E_{BGC}, obtained from the DFT calculation on the Hg-compound surfaces, with the band gap E_g, obtained from the G_0W_0 result on the bulk, to calculate the VBM and

conduction band minimum (CBM), in the following manner:[40]

$$E_{\mathrm{VBM}} = E_{\mathrm{BGC}} - \frac{1}{2}E_g^{\mathrm{GW}}, \;\; E_{\mathrm{CBM}} = E_{\mathrm{BGC}} + \frac{1}{2}E_g^{\mathrm{GW}}. \quad (1)$$

The corrected band edges can thus be compared with possible reduction/oxidation processes induced by the interaction with light and the presence of halogens at the surface of the minerals.

3 RESULTS

3.1 X-ray analyses

The mineral composition in samples of paintings exhibiting different degradation levels has been studied in previous works through XANES measurements.[10–12] Confirmation of the composition can ultimately be achieved by comparing our theoretical XANES spectra with experimental spectra obtained on reference compounds, as shown in Fig. 1. Reference data are reproduced from previous works.[10–12] The computed S K edge spectrum of pure red α-HgS, shown in Fig. 1(a), is in excellent agreement with the reference data, as well as with measurements on the undamaged pigment (Fig. 9(b) of Ref.,[12] not shown here). Computed Cl K edge spectra of the mercury sulfochlorides are reported in panel (b). In the absence of reference spectra for all compounds, we show only that of the α-phase, corderoite, for comparison. The theoretical spectrum of α-$Hg_3S_2Cl_2$ reproduces well the observed double-peak structure at low energy as well as the broader feature at 2.836 keV. The γ-phase (kenhsuite) curve is quite similar to that of the α-polymorph, although the main feature at 2.826 keV is more intense in this case. The spectrum for the third (less stable) polymorph (β-$Hg_3S_2Cl_2$) is also shown. Its presence has not been reported (yet) in experiments, and thus we show the data only as a reference for further investigations. The main difference with the other two polymorphs is in a slight shift to lower energies of the third (broader) spectra feature, and the complete absence of any structure at 2.823 keV. Both mercury chlorides (panels (c) and (d)) are also in excellent agreement with the reference curves and are

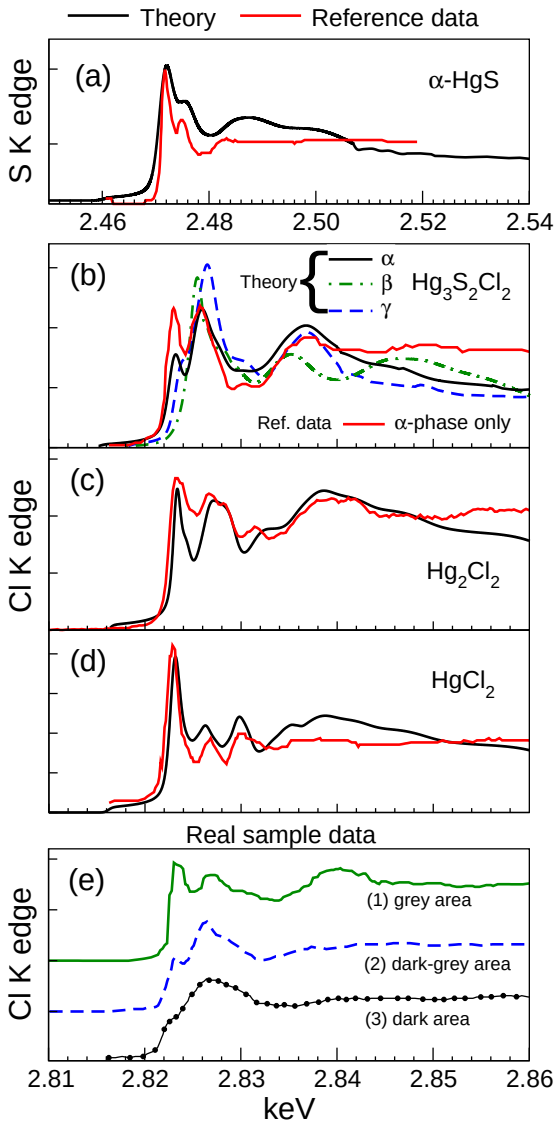

Figure 1: Computed XANES spectra for α-HgS (a), α-, β-, and γ- $Hg_3S_2Cl_2$ (b), Hg_2Cl_2 (c), and $HgCl_2$ (d), compared with experimental data taken from reference compounds. Panel (b) reports reference data for α-$Hg_3S_2Cl_2$ only. Spectra shown in panel (e) are previously measured data from actual samples of degraded vermilion (see text for details and references).

both characterized by strong sharp peaks at 2.823 keV. Hg_2Cl_2 (calomel) also exhibits a strong distinguishing feature around 2.828 keV. In summary, therefore, the agreement between the computed and reference data for each material is, on the whole, very good, demonstrating that the theory at the DFT level is well able to reproduce the spectral

features and their positions.

Let us now discuss XANES spectral features measured on real samples of degraded vermilion as reported elsewhere.[10–12] Fig. 1(e) shows characteristic Cl K edge spectra obtained from a variety of sources: (1) a thin light-grey layer found covering α-HgS grains on a wall painting at the Monastery of Pedralbes in Barcelona, Spain (Cotte *et al.*, Ref.[11]); (2) a dark-grey spot on a sample from a Pompeian wall painting (Cotte *et al.*, Ref.[10]); and (3) the corner of a badly degraded sample of the *Adoration of the Magi* by P. P. Rubens (Radepont *et al.*, Ref.[12]). For a thorough treatment, one should compare these spectra with linear combinations of various reference spectra (which is indeed done in experimental works). Here we limit ourselves to a qualitative analysis by pointing out the main common aspects between the measured data and our computed spectra. For further detail on the experimental measurements we refer the reader to the original works.

The spectra of degraded areas exhibiting a lighter colour (1) are characterized by strong, comparable spectral features at 2.823 and 2.827 keV, and a distinct broad hump around 2.840 keV. As already noted in Ref.,[11] this matches extremely well with the XANES profile of Hg_2Cl_2, and supports its presence in the whitish areas of the samples, which are also reported to have a higher relative concentration of Cl.[12,20] Of course, this doesn't exclude the presence of other species in this region: α-$Hg_3S_2Cl_2$ (and, to a lesser extent, $HgCl_2$) also has peaks near these energies, although the lineshape is quite different.

XANES spectra from the darker areas of the paintings [(2) and (3)] are instead characterized by a dominant broad feature around 2.826 keV and a weaker one at 2.823 keV. This lineshape is thus reproduced well by our calculated spectrum of α-$Hg_3S_2Cl_2$ (solid black curve, Fig. 1(b)). The presence of γ-$Hg_3S_2Cl_2$ cannot be excluded on the basis of our results, which rely on electronic structure properties and which do not include thermochemistry details. Last we note that the mercury chlorides also show a peak at 2.823 keV. As shown below, however, their presence in a darkly coloured area is unlikely.

In conclusion, our X-ray spectra confirm the experimental observations of specific

	DFT (AE)	DFT (PSP)	G_0W_0 (PSP)	Exp.
α-HgS cinnabar (indirect)	1.41	1.40	2.24	2.1–2.28 (Refs. [42–44]);
(direct)	1.42	1.42	2.43	
Hg_2Cl_2 calomel	2.12	2.06	3.52	4.39, 3.9 (Refs. [45,46])
$HgCl_2$ mercuric chloride	3.10	3.00	5.43	
α-$Hg_3S_2Cl_2$ corderoite	2.09	1.98	2.90	

Table 1: Band gaps of mercury compounds at the DFT level obtained by the all electron (AE) and pseudopotential (PSP) approaches, at the G_0W_0 level, and experimental data. All energies are expressed in eV.

chemical species present in paintings in regions of different degradation levels. It seems certain that the colour-change phenomenon involves minerals with different structural and optical properties, suggesting that a complex transformation sequence is taking place.

3.2 Electronic and optical properties

In our previous work [27] we presented the band gaps of α-HgS, α-$Hg_3S_2Cl_2$ and Hg_2Cl_2 as obtained from a G_0W_0 calculation in a pseudopotential approach. Here we present a more detailed analysis of the electronic and optical properties of the various materials (also including the sometimes observed mercuric chloride, $HgCl_2$), compare all-electron with pseudopotential results, and present the anisotropic optical properties of the main, original red α-HgS.

In Table 1 we report the band gaps of all compounds obtained using DFT with different approaches. The very good agreement between the DFT all electron (AE) results and those obtained with a DFT pseudopotential (PSP) approach is excellent for all compounds, making us confident that the X-ray analysis presented above (based on an AE approach) and the electronic/optical analysis presented below (in a PSP approach) rely on the same, consistent, ground state description of the systems within DFT. Previously we concluded that computed band edge positions do not support the dissociation of HgS into Hg and S through reduction of Hg^{2+} by photoexcited electrons entering the HgS conduction band, a finding in agreement with experimental studies. [41] We thus provide firmer proof that the band edges of α-HgS used in that discussion were correctly estimated.

Table 1 also demonstrates that our results for α-HgS (2.24 eV for the indirect gap) are in excellent agreement with the experimental values from photoemission experiments at 300 K as well as with those from optical measurements (reporting an indirect band gap of 2.28 eV at liquid helium temperatures, 2.225 eV at liquid nitrogen temperatures, and 2.1 eV at room temperature[42–44]). Although in principle our G_0W_0 results do not give access to optical properties (due to the neglect of particle-hole excitations), such favorable comparison suggests that excitonic coupling does not lead to a large difference between the electronic and optical gaps, and thus that excitonic effects in this compound are relatively small, confirming previous experimental findings.[47] However, from the theoretical point of view, identification of a material's colour requires a calculation of its optical absorption spectrum, whose onset is determined by the optical band gap and which is accessible only by going beyond a single (quasi-) particle perturbative approach through solution of the Bethe-Salpeter equation (BSE).

In Fig. 2 we show the optical response of α-HgS with the electric field of the light parallel and perpendicular to the trigonal axis of the system (ordinary ray and extraordinary ray), calculated in DFT (RPA, independent particle picture), G_0W_0 and G_0W_0+BSE. Apart from the higher intensity of the absorption for the electric field parallel to the trigonal axis,[48] we observe that in both cases the BSE spectra brings a remarkable change in the spectral weight. Nevertheless, and more importantly, the behaviour in terms of the excitonic shift as brought by the BSE results with respect to the G_0W_0 one is similar for both two rays: the onset of absorption in the two MBPT approaches differ by $\sim$0.2 eV (i.e., the *GW* and optical gaps are very close). We thus conclude that the G_0W_0 gap well describes the colour of our system, which is due to a ligand-to-metal charge transfer transition with the 6*s* orbital as acceptor.

G_0W_0 results are also reported in Table 1 for the other mercury compounds. The results for α-$Hg_3S_2Cl_2$ (2.90 eV) and Hg_2Cl_2 (3.52 eV) were already reported in our previous work.[27] Without taking into account possible excitonic effects, the band gap of α-$Hg_3S_2Cl_2$ suggests a white-yellowish colour, in perfect agreement with observations.[12,22] A first comparison between our G_0W_0 results for Hg_2Cl_2 with optical absorption data at low temperatures gives excellent agreement (4.39 eV at 100 K[45]) and

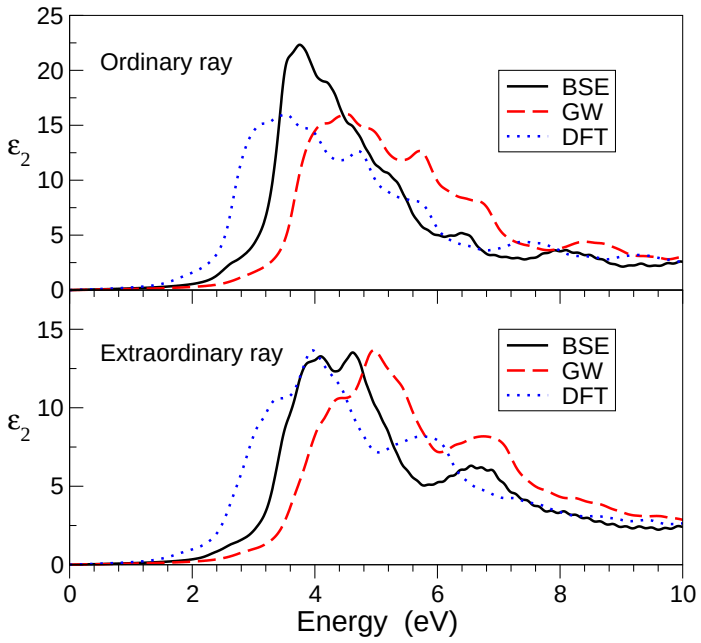

Figure 2: The optical absorption of α-HgS for electric field of the light perpendicular to the c axis (extraordinary ray) and parallel to the c axis (ordinary ray), computed within the DFT, GW and BSE methods.

suggests a temperature-dependent formation of excitons when comparing with room-temperature data (3.9 at 298 K[46]), which nevertheless leave the system uncoloured. The value of our band gap explains the transparency of the material to visible light and thus its white colour. Kenhsuite turns out to be metallic at the DFT level, and thus remains so in the first order perturbative approach. We cannot exclude that at the specific temperature/pressure conditions in which this mineral is formed, the covalency could change and a gap could be opened. Kenhsuite is reported to have a canary or straw yellow colour.[49] Finally, the band gap of $HgCl_2$ results to be 5.43 eV, very far from the visible light region. According to our analysis at $T = 0$, and assuming similarly weak excitonic effects for all Hg-bearing compounds analyzed here, a schematic picture of the correspondance of the G_0W_0 (quasiparticle) gap—and hence, the onset of absorption—with the *observed* colours of the minerals can be deduced: this is reported in Fig. 3.

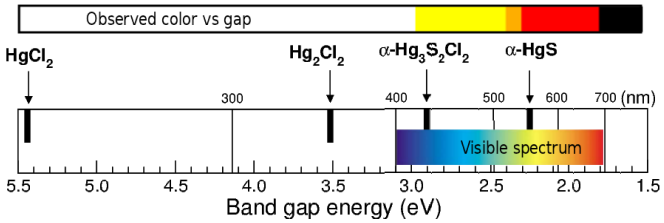

Figure 3: Schematic correspondance between the G_0W_0 gaps and the observed colours of the four minerals studied in this work (assuming weak excitonic effects).

3.3 Growth of secondary minerals: the role of chloride

What triggers the transformation sequence? Chloride pollutants, common in humid environments and present even in the protective punix wax,[10] have been shown to play a relevant role in the darkening process of α-HgS. Cl can readily chemisorb to the α-HgS surface via direct oxidation from the photoinduced valence band holes in α-HgS.[27] Here we provide details about our study of chemisorption geometries.

A structure and topology analysis supports a photoinduced, chloride-driven growth of secondary minerals, with bonding environments similar to those present in α-HgS. Within DFT, we find that Cl adsorb at the cleavage $(10\bar{1}0)$ surface of α-HgS at a bridging site between parallel S-Hg-S chains (see Fig. 4(a); adsorption energy = 1.52 eV). The Hg–Cl interatomic distance (2.88–2.93Å) is consistent with the equivalent (bridging) distances found in β-$Hg_3S_2Cl_2$ (2.83Å), γ-$Hg_3S_2Cl_2$ (2.84Å) and α-$Hg_3S_2Cl_2$ (2.87Å) (Fig. 4(b) and (c)). Similar observations can be made for the S–Cl distances (α-HgS/Cl: 3.85–3.99Å; α-$Hg_3S_2Cl_2$: 3.72–4.03Å; γ-$Hg_3S_2Cl_2$: 3.90–3.93Å). Chloride thus adsorbs into geometries that could indeed seed the growth of layers with bonding environments compatible with the new Hg-S-Cl-containing phases, which supports the observations[12,22,49] that α-HgS (non-cubic) may be transformed into different sulfochloride minerals before finally ending up as the more stable cubic α-$Hg_3S_2Cl_2$. In contrast, Hg-Cl distances in e.g. Hg_2Cl_2 are much smaller (2.52Å), indicating a very different bonding environment.

Inspection of the 3D topology also supports the reported superficial formation of α-$Hg_3S_2Cl_2$. As shown in Fig. 4(d), α-$Hg_3S_2Cl_2$ appears to offer the most natural

and optimal transformation of the underlying α-HgS: both minerals are composed of parallel helical -Hg-S-Hg- structures having the same natural width and chirality, although the spatial periods differ slightly. In α-$Hg_3S_2Cl_2$, these helices are further cross-linked via S-Hg-S bridges into a spatial framework with Cl atoms lying in the cavities. Fig. 4(d) shows that the HgS helical chains constitute a natural basis for matching the α-HgS and α-$Hg_3S_2Cl_2$ lattices, while Cl atoms adsorbed at the α-HgS $(10\bar{1}0)$ bridge sites also coincide with their positions in α-$Hg_3S_2Cl_2$. The adsorbed weakly bound halide ions can adapt easily in the α-HgS lattice due to the fact that they are not involved in strictly oriented chemical bonding (contrary to the covalently bound chalcogen ions).[31] These results supports previous experimental findings where small quantities of poorly crystalline white-yellowish α-$Hg_3S_2Cl_2$ were shown to be formed from α-HgS in the presence of ions common in natural waters and in an acid environment, as given by the presence of NaCl and HCl.[22,49,50] Early thermochemical estimations[51] predicted its formation and stability to be possible only at a pH around 2.

3.4 Light-induced structural instability of defective α-$Hg_3S_2Cl_2$ and degradation of chloride phases

In order to determine whether light-induced degradation phenomena can occur in the secondary minerals under simultaneous exposure to air, we need to study if changes of their structural properties and/or if (photo)chemical processes are possible. In our previous work, we claimed that α-$Hg_3S_2Cl_2$ is unstable under light illumination. Here we provide further details about our analysis. We also present a possible degradation mechanism for $HgCl_2$, which is observed on certain paintings, and which was not analyzed before.

The presence of different types of defects induced by exposure to air can introduce new states in the band gap of the mineral, change the band gap itself, or change the nature of the states at the band edges. For the case of a S vacancy, as suggested by several experiments,[10,12] it is possible to observe such changes by looking at the comparison between the density of states (DOS) of the pure and defective system, especially in

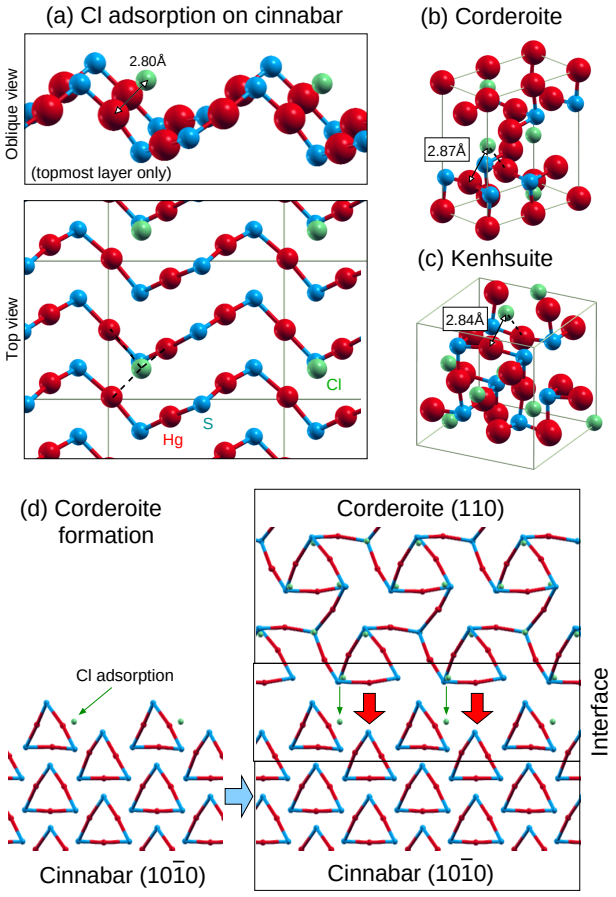

Figure 4: Cl adsorption geometry (side and top views) on cinnabar (α-HgS) (a); Hg–Cl atomic distances in (b) corderoite (α-$Hg_3S_2Cl_2$) and (c) kenhsuite (γ-$Hg_3S_2Cl_2$); and proposed interface between corderoite and cinnabar (d).

angular-momentum resolved mode (projected partial density of states), as reported in Fig. 5. The DOS for the defective structure shows no real change in terms of a red-shift of the band gap, but instead indicates a change in the nature of the states at the band edges of the system.

Pure α-$Hg_3S_2Cl_2$ has a direct band gap at the center of the Brillouin zone. The valence band at the BZ center has a large contribution from Cl ions, but strong mixing of Cl, S, and Hg states does occur at general points in the Brillouin zone. In the conduction region the Hg 6*s* and 6*p* states are mixed with strong contributions from the sulfur, but the situation changes upon formation of the planar triangular Hg_3 cationic

cluster that is created when one S atom is released, according to our DFT structural optimization of the defective α-$Hg_3S_2Cl_2$. In such defective structures, the dominant contribution at the conduction band minimum is given by Hg *s*-states, which appear to have little dispersion.

For these planar triangular clusters, strong distortions and release of Hg ions have been reported. Indeed, although our calculations do not include relativistic effects, it is known that the bonding between mercury ions is intriguing: the relativistic contraction of its atomic orbitals makes it behave chemically almost like a noble gas, not wanting to share electrons even with other mercury atoms. The relativistic stabilization of the Hg 6*s* orbital provides an energetic advantage when two Hg^+ ions share a pair of 6*s* electrons which results in the relatively stable Hg_2^{2+} ion, in which Hg has a (I) oxidation state.[52] Regarding our results, crystal field and molecular orbital theory allows us to analyze the symmetry of states: the bonding within the Hg_3^{4+} cluster in D_{3h} symmetry can be considered as given by the (weak) overlap of the *s* orbital, which generates a bonding a_1' and two degenerate weakly antibonding orbitals e'. Since nature avoids degeneracy, a distortion (Jahn Teller mechanism, JT) is expected when photoexcited electrons occupies such degenerate levels. Trimeric fragments of Hg_3^{4+} in their excited state disproportionate under photolysis and eventually release Hg atoms[53–56] to reduce the strain energy in the lattice, although a long exposure[54–56] is needed to dissociate the fragment, with release of one Hg atom and stabilization of dimeric H_2^{2+} units.[52,57] An *ab-initio* approach for the JT mechanism is not yet available and will surely be a major challenge. However, we have previously shown[27] that the energy to emit one of the Hg atoms from the JT active fragment is 1.82 eV, perfectly compatible with both visible sunlight and museum lamps. The formation of defects in α-$Hg_3S_2Cl_2$, due both to its imperfect growth on the α-HgS surface and to its exposure to contaminants, triggers the darkening process via release of grey-dull elemental Hg(0). The concomitant formation of dimeric H_2^{2+} units provides a natural explanation for the formation of Hg_2Cl_2, eventually giving rise to the observed whitish streaks.

Some authors have suggested that α-$Hg_3S_2Cl_2$ dissociates partially into elemental Hg(0), S, and mercury chloride compounds (Hg_2Cl_2 and then to $HgCl_2$);[13] others that

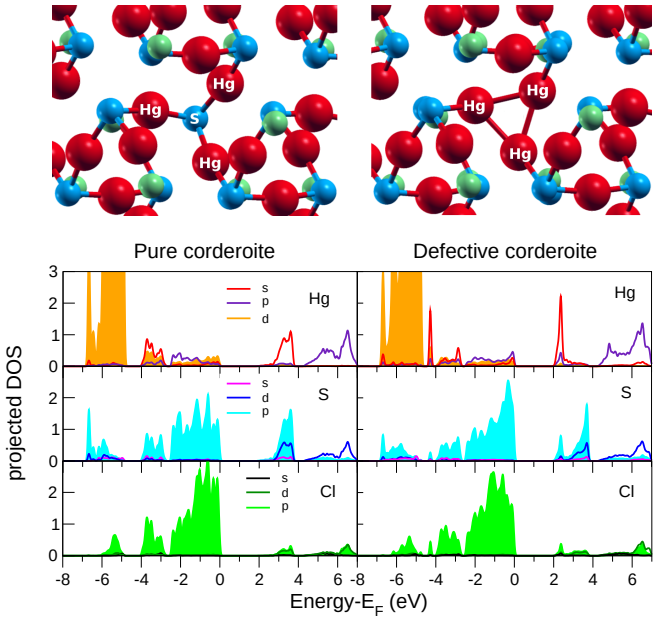

Figure 5: Local atomic structure (top) and projected partial density of states (bottom) for pure α-$Hg_3S_2Cl_2$ (left) and defective α-$Hg_3S_2Cl_2$ with a S vacancy (right).

it dissociates to elemental S, HgS, and Hg_2Cl_2.[10,20] Experiments on the photolysis of $HgCl_2$ show the reduction of the metal center with the formation of insoluble Hg_2Cl_2.[58] Though some kinetic modelling would be needed in order to determine the fastest and more favourable path of dissociation for α-$Hg_3S_2Cl_2$, our X-ray results support the idea that Hg_2Cl_2 is the main component in the white areas of the paintings, suggesting that a higher Cl amount and a longer exposure to light is ultimately needed to form Hg_2Cl_2. In some of the paintings, the white streaks have been observed to be constituted only by Hg_2Cl_2, while in other cases also $HgCl_2$ was observed. In the following, we analyze the possibility of degradation of the latter compound via electron transfer processes, calculating its band edges and comparing them with relevant redox reactions which could eventually lead to photoreduction of the Hg ions and their deposition on the surface of the mineral.[41]

The DFT-GGA band structure of the $HgCl_2$(100) surface is reported in Fig. 6. There are no defect or surface states within the gap, and therefore the slab band gap is close to that of the bulk (∼3.0 eV). This allows us to use our approximate *GW* scheme to

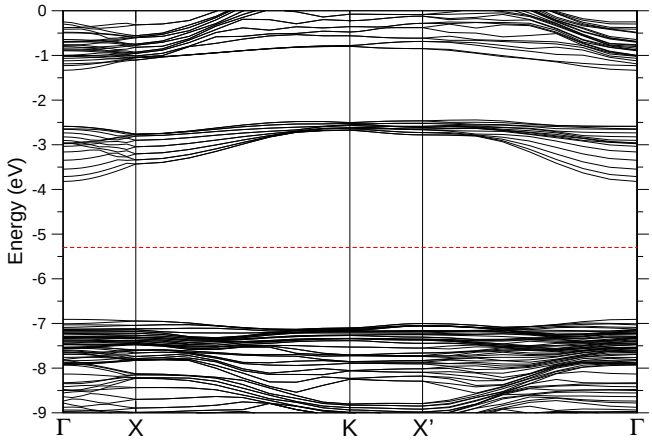

Figure 6: DFT band structure of the $HgCl_2(100)$ surface, relative to the vacuum level. The Fermi level is indicated.

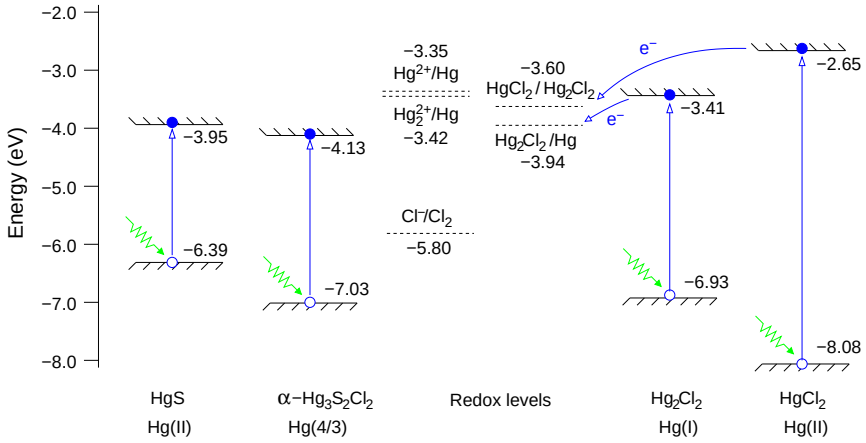

Figure 7: Band levels of the materials studied in this work, compared with standard Hg-relevant redox levels. Possible direct photoreduction processes in $HgCl_2$ and Hg_2Cl_2 are indicated.

renormalize the band edges, as described previously. Corrected band edges are reported in Fig. 7 for $HgCl_2$, where they are compared with relevant redox reactions involving the Hg ions. For completeness, we also show the band edges of α-HgS, α-$Hg_3S_2Cl_2$, and Hg_2Cl_2, as reported in our previous work.[27] We observe that, similar to the Hg_2Cl_2 case, photoirradiation can induce a chemically-driven partial decomposition of $HgCl_2$ via electron transfer.

4 Conclusions

This work constitutes a solid step towards the understanding of degradation phenomena of mercury compounds in artworks which are exposed to light, humidity and common contaminants or pollutants (chlorides, in particular) that are present in air. The fundamental mechanisms involved in the darkening of α-HgS reveal the important roles played by light and halogens, both common to humid environments, and highlights the physical and chemical origins of the degradation processes. Such analysis holds much promise and paves the way for further applications of these methods for the advancement of the field.

Ab-initio calculations of XANES spectra for various chlorides and sulfochlorides of mercury, taken in combination with predictions of their colour (obtained using state-of-the-art quasiparticle methods), provide valuable information concerning their presence in dark and/or light regions of degraded vermilion. Our calculations predict that the secondary mineral γ-$Hg_3S_2Cl_2$ is coloured, for instance, which is not consistent with the hypothesis[12] that its colocalization with the darker area is only apparent. It is thus possible that, during the degradation process, the non-cubic α-HgS is transformed into the non-cubic γ-$Hg_3S_2Cl_2$ phase first and then to the most stable cubic sulfochloride phases (α and β), as observed and suggested by several experiments[22,49] who reported α-$Hg_3S_2Cl_2$ formation from α-HgS.

Accurate calculations of the absolute band edge positions are obtained by combining these quasiparticle calculations with DFT simulations that take into account the surface or interface geometry. The computed band edges can then be compared with possible reduction/oxidation effects induced by the interaction with light and the presence of chloride contaminants, and allows us to rule out direct photoreduction of α-HgS. Instead, we propose a mechanism in which α-$Hg_3S_2Cl_2$ plays a key role, and provide evidence to support its growth at the α-HgS surface following chlorine adsorption. Formation of trimeric Hg_3^{4+} fragments inside the sulfochloride becomes unstable under illumination and provide a natural pathway for precipitation of elemental Hg, ultimately responsible for the observed darkening, as well as formation of mercury chlo-

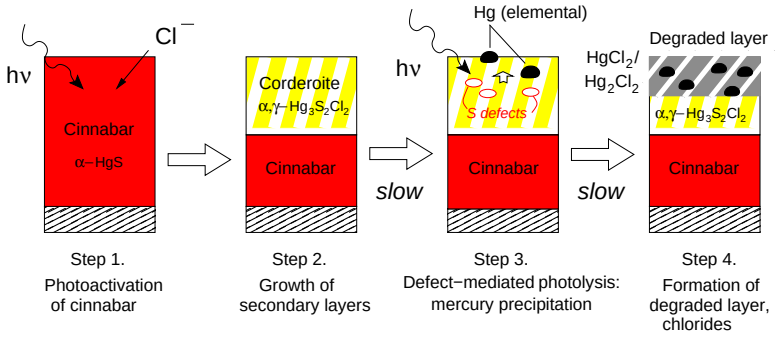

Figure 8: Schematic overview of the degradation process (see text).

rides. The computed electronic levels for the most likely exposed surfaces of Hg_2Cl_2 and $HgCl_2$ align favorably with the potential for reduction of Hg (eventually to elemental Hg), allowing for further photo-induced direct deposition mechanisms on the surface of the pigment.[41] Our results support a more favourable electron transfer mechanism for $HgCl_2$ than for Hg_2Cl_2, suggesting that it degrades more rapidly. Together with the reported[57] higher stability of Hg_2Cl_2 with respect to $HgCl_2$, this explains why the presence of the latter varies from sample to sample, in contrast to the ubiquity of the other species. More advanced studies taking into account possible slight shifts of the band edges due to a more accurate alignment for solids immersed in solutions[59,60] are needed to confirm these conclusions, but we expect that they would leave the order of the band edges for the minerals unaffected.

A schematic overview of the proposed degradation process is thus reported in Fig. 8. At first, under the effect of light and in the presence of humidity, Cl adsorbs on the α-HgS surface and triggers the growth of a secondary mineral (α-$Hg_3S_2Cl_2$), whose lattice topology resembles that of the underlying α-HgS. The lack of perfect lattice matching between α-$Hg_3S_2Cl_2$ and α-HgS, combined with the exposure to air pollutants and to illumination by light, facilitates the subsequent formation of structural instabilities within the secondary material. These instabilities (S vacancies, formation and dissociation of trimeric Hg_3^{4+} fragments) lead to the release of grey elemental Hg(0) precipitating on the pigment surface, as well as the formation of other (pure) chloride phases that produce grey/white streaks on the darkened vermilion. As

our calculations show, these chloride phases are also subject to further degradation via photoelectron transfer processes which occur according to their (different) energy barriers, providing a second channel for Hg(0) precipitation.

We suggest that experimentalists perform luminescence/Raman measurements of pure and degraded α-$Hg_3S_2Cl_2$ with both solar simulators and monochromatic UV light in order to elucidate the decay mechanism and clarify the role of defects and contaminants (concentration, defect-assisted self-trapping of photoinduced carriers, etc.). Our study thus implies that, while works of art such as outdoor mural paintings can hardly be protected, degradation of indoor paintings in museums can be avoided with continuous control of the humidity and chloride levels in the air and by using below-gap illumination of the paintworks. The methodology followed in this work could equally well be applied to the problem of degradation in other pigments, and may help in assessing the viability of innovative restoration procedures.

5 Acknowledgments

The authors acknowledge the CINECA award under the ISCRA initiative, for the availability of high performance computing resources and support. F. Da Pieve acknowledges the Consortium des Équipements de Calcul Intensif (CÉCI), funded by the Fonds de la Recherche Scientifique de Belgique (F.R.S.-FNRS) under Grant No. 2.5020.11 for the availability of computational resources and support. F. Da Pieve acknowledges financial support from the European Community under a Marie Curie Intra-European Fellowship (Programme FP7/2007-2013), the host group, Laboratoire des Solides Irradiés, École Polytechnique, Palaiseau, France and kind hospitability from ULB, Free University of Brussels, Belgium during the first part of this project.

6 Appendix: Plasmon-pole approximations in GW calculations

We briefly recall here the main ingredients of MBPT in the *GW* approximation. The key quantity for the correction of the DFT values is the self-energy operator, which contains the information related to the many body interactions between electrons, and which is constructed as the convolution of the one-particle Green's function G and the screened Coulomb interaction W:

$$\Sigma(r,r';\omega) = \frac{i}{2\pi}\int_{-\infty}^{\infty} d\omega' G(r,r';\omega+\omega')W(r,r';\omega').$$

The initial Green's function G is constructed using Kohn-Sham orbitals and energies, and W is given by:

$$W(r,r';\omega) = \int dr'' \varepsilon^{-1}(r,r'';\omega)v(r'',r') \tag{2}$$

where $\varepsilon(r,r'';\omega)$ is the frequency dependent dielectric function and $v(r'',r')$ the bare Coulomb interaction. In principle, the *GW* equations should be iterated to self-consistency, but as a practical approach the self-energy corrections are often calculated in a single iteration in a perturbative manner (this is called one-shot *GW* or G_0W_0).

Calculation of the dielectric function represents a crucial step in the evaluation of the self energy. It must be computed to a high precision, and often causes a bottleneck in numerical simulations. In order to account for full frequency dependence the contour deformation technique (CD), which deforms the integration path, can be used.[61] However, in practical applications, the frequency dependence of the imaginary part of ε^{-1} is assumed to be well described by a delta function within the so-called plasmon-pole (PP) models. These models posit an analytical frequency behavior and thus remove the need for a costly numerical integration. The plasmon-pole model parameters are determined in order to reproduce the behavior of the dielectric matrix in the static limit

	E_g^{ind} (eV)	E_g^{dir} (eV)	ΔE_{VBM}	ΔE_{CBM}
DFT-GGA	1.41	1.42	0.00	0.00
CD	2.25	2.38	−0.39	+0.64
GN PP	2.24	2.43	−0.34	+0.56
HL PP	2.30	2.49	−0.64	+0.35

Table 2: Computed DFT-GGA and G_0W_0 results for the indirect and direct band gaps of α-HgS, as well as G_0W_0 corrections to the DFT valence band maximum (VBM) and conduction band minimum (CBM). CD, GN and HL refer to the use of the contour deformation technique and Godby-Needs and Hybertsen-Louie plasmon-pole (PP) models, respectively, in the G_0W_0 calculation (see text). All energies are in eV.

($\omega = 0^+$). Additionally, in the Godby-Needs (GN) PP model[62] one more frequency along the imaginary axis $i\omega_p$ near the plasma frequency is used to fix the parameters, while in other PP models, like the Hybertsen and Louie (HL) PP model,[63] the parameters are determined by forcing the dielectric function to fulfill the so-called f-sum rule.[64]

Since many-body corrections depend on an accurate treatment of the frequency dependence of the dielectric function, different estimations of the band gap E_g can considerably influence the final values of the absolute band edge positions through Eq. 1. We have carefully checked the estimation of band gaps in α-HgS (cinnabar) by comparing the values obtained by taking into account full frequency dependence in the self-energy operator (CD approach) with results from the GN PP and HL PP models. As shown in Table 2, self-energy corrections obtained with the CD approach open the gap to 2.25 eV (direct) and 2.38 eV (indirect). Within the GN PP model G_0W_0 gaps are 2.24 and 2.43 eV, while using the HL PP model we obtain 2.30 and 2.49 eV. The GN PP results thus appear slightly closer to the CD results. The superior performance of the GN PP model has already been noted elsewhere in quite different systems (e.g. zinc oxide[65]) and is explained by the fact that the enforcement of the sum rule in the HL model can push the Dirac delta peak of the imaginary part of the dielectric function to unphysical values. This results in an overestimation of the pole contribution along the imaginary axis, in particular for the low frequency region.

The good performance of the GN PP model can also be checked by looking at the band edge positions. Table 2 also reports the G_0W_0 corrections to the VBM and

CBM for α-HgS according to the CD, GN PP and HL PP models. We observe that the variation of such corrections in the two PP models is such that the HL results pushes the VBM to lower energies and the CBM is shifted less with respect to the trend given by the GN PP model, the latter giving a much better agreement with the CD results. Hence, although the error in the band gaps is of the order of 0.1 eV, the error in the absolute band positions is substantially larger, ~ 0.3 eV.

All PP calculations appearing in the main text have therefore been computed using the GN PP model.

References

[1] L. Zanella, F. Casadio, K. A. Gray, R. Warta, Q. Ma and J.-F. Gaillard, *Journal of Analytical Atomic Spectrometry*, 2011, **26**, 1090.

[2] C. Gervais, M.-A. Languille, S. Réguer, M. Gillet, S. Pelletier, C. Garnier, E. P. Vicenzi and L. Bertrand, *Journal of Analytical Atomic Spectrometry*, 2013, **28**, 1600.

[3] L. Samain, B. Gilbert, F. Grandjean, G. J. Long and D. Strivay, *Journal of Analytical Atomic Spectrometry*, 2013, **28**, 524.

[4] E. Del Federico, W. Shöfberger, J. Schelvis, S. Kapetanaki, L. Tyne and A. Jerschow, *Inorganic chemistry*, 2006, **45**, 1270–6.

[5] S. Fantacci, A. Amat and A. Sgamellotti, *Accounts of chemical research*, 2010, **43**, 802–13.

[6] A. Tilocca and E. Fois, *The Journal of Physical Chemistry C*, 2009, **113**, 8683–8687.

[7] I. Cianchetta, I. Colantoni, F. Talarico, F. D'Acapito, A. Trapananti, C. Maurizio, S. Fantacci and I. Davoli, *Journal of Analytical Atomic Spectrometry*, 2012, **27**, 1941.

[8] A. M. Conte, O. Pulci, M. C. Misiti, J. Lojewska, L. Teodonio, C. Violante and M. Missori, *Applied Physics Letters*, 2014, **104**, 224101.

[9] A. Romani, C. Clementi, C. Miliani and G. Favaro, *Photochemistry*, 2011, **39**, 256–284.

[10] M. Cotte, J. Susini, N. Metrich, A. Moscato, C. Gratziu, A. Bertagnini and M. Pagano, *Analytical chemistry*, 2006, **78**, 7484–92.

[11] M. Cotte, J. Susini, V. A. Solé, Y. Taniguchi, J. Chillida, E. Checroun and P. Walter, *Journal of Analytical Atomic Spectrometry*, 2008, **23**, 820.

[12] M. Radepont, W. de Nolf, K. Janssens, G. Van der Snickt, Y. Coquinot, L. Klaassen and M. Cotte, *Journal of Analytical Atomic Spectrometry*, 2011, **26**, 959.

[13] K. Keune and J. J. Boon, *Analytical chemistry*, 2005, **77**, 4742–50.

[14] P. Vandenabeele, K. Lambert, S. Matthys, W. Schudel, A. Bergmans and L. Moens, *Analytical and bioanalytical chemistry*, 2005, **383**, 707–12.

[15] J. K. McCormack, *Mineralium Deposita*, 2000, **35**, 796–798.

[16] R. S. Davidson, C. J. Willsher and C. L. Morrison, *Journal of the Chemical Society, Faraday Transactions 1: Physical Chemistry in Condensed Phases*, 1982, **78**, 1011.

[17] J. K. McCormack, F. W. Dickson and M. P. Leshendok, *American Mineralogist*, 1991, **76**, 1715–1721.

[18] R. S. Davidson and C. J. Willsher, *Journal of the Chemical Society, Dalton Transactions*, 1981, 833.

[19] R. J. Gettens, R. L. Feller and W. Chase, in *Artists' Pigments: A Handbook of their History and Characteristics, Volume 2*, ed. A. Roy, Oxford University Press, Oxford, 1993, pp. 159–182.

[20] M. Spring and R. Grout, *National Gallery Technical Bulletin*, 2002, **23**, 50.

[21] A. Deneckere, W. Schudel, M. Van Bos, H. Wouters, A. Bergmans, P. Vandenabeele and L. Moens, *Spectrochimica acta. Part A, Molecular and biomolecular spectroscopy*, 2010, **75**, 511–9.

[22] E. Foord, P. Berendsen and L. O. Storey, *American Mineralogist*, 1974, **59**, 652–655.

[23] J. K. McCormack and F. W. Dickson, *The Canadian Mineralogist*, 1998, **36**, 201–206.

[24] E. L. Kendix, S. Prati, E. Joseph, G. Sciutto and R. Mazzeo, *Analytical and bioanalytical chemistry*, 2009, **394**, 1023–32.

[25] R. J. H. Clark, P. J. Gibbs, K. R. Seddon, N. M. Brovenko and Y. A. Petrosyan, *Journal of Raman Spectroscopy*, 1997, **28**, 91–94.

[26] R. Fuchs, in *Art 2002: 7th International Conference on Non-destructive Testing and Microanalysis for the Diagnostics and Conservation of the Cultural and Environmental Heritage*, 2002.

[27] F. Da Pieve, C. Hogan, D. Lamoen, J. Verbeeck, F. Vanmeert, M. Radepont, M. Cotte, K. Janssens, X. Gonze and G. Van Tendeloo, *Physical Review Letters*, 2013, **111**, 208302.

[28] W. Anaf, K. Janssens and K. De Wael, *Angewandte Chemie (International ed. in English)*, 2013, **52**, 12568–71.

[29] R. M. Dreyer, *American Mineralogist*, 1938, **23**, 457–460.

[30] W. G. Aulbur, L. Jönsson and J. W. Wilkins, *Solid State Physics*, 1999, **54**, 1–218.

[31] S. A. Magarill, N. V. Pervukhina, S. V. Borisov and N. A. Pal'chik, *Russian Chemical Reviews*, 2007, **76**, 101–131.

[32] J. P. Perdew, K. Burke and M. Ernzerhof, *Physical Review Letters*, 1996, **77**, 3865–3868.

[33] P. Blaha, K. Schwarz and G. Madsen, *WIEN2K, An Augmented Plane Wave+ Local Orbitals Program for Calculating Crystal Properties*, TU Wien, Austria, 2001.

[34] J. J. Rehr, J. A. Soininen and E. L. Shirley, *Physica Scripta*, 2005, **2005**, 207.

[35] X. Gonze, B. Amadon, P.-M. Anglade, J.-M. Beuken, F. Bottin, P. Boulanger, F. Bruneval, D. Caliste, R. Caracas, M. Côté, T. Deutsch, L. Genovese, P. Ghosez, M. Giantomassi, S. Goedecker, D. Hamann, P. Hermet, F. Jollet, G. Jomard, S. Leroux, M. Mancini, S. Mazevet, M. Oliveira, G. Onida, Y. Pouillon, T. Rangel, G.-M. Rignanese, D. Sangalli, R. Shaltaf, M. Torrent, M. Verstraete, G. Zerah and J. Zwanziger, *Computer Physics Communications*, 2009, **180**, 2582–2615.

[36] P. Giannozzi, S. Baroni, N. Bonini, M. Calandra, R. Car, C. Cavazzoni, D. Ceresoli, G. L. Chiarotti, M. Cococcioni, I. Dabo, A. Dal Corso, S. de Gironcoli, S. Fabris, G. Fratesi, R. Gebauer, U. Gerstmann, C. Gougoussis, A. Kokalj, M. Lazzeri, L. Martin-Samos, N. Marzari, F. Mauri, R. Mazzarello, S. Paolini, A. Pasquarello, L. Paulatto, C. Sbraccia, S. Scandolo, G. Sclauzero, A. P. Seitsonen, A. Smogunov, P. Umari and R. M. Wentzcovitch, *Journal of Physics. Condensed Matter*, 2009, **21**, 395502.

[37] F. Da Pieve, M. Stankowski and C. Hogan, *Science of the Total Environment*, 2014, **493**, 596–605.

[38] J. Perdew and M. Levy, *Physical Review Letters*, 1983, **51**, 1884–1887.

[39] J. Janak, *Physical Review B*, 1978, **18**, 7165–7168.

[40] M. C. Toroker, D. K. Kanan, N. Alidoust, L. Y. Isseroff, P. Liao and E. a. Carter, *Physical Chemistry Chemical Physics*, 2011, **13**, 16644–54.

[41] B. Pal, S. Ikeda and B. Ohtani, *Inorganic chemistry*, 2003, **42**, 1518–24.

[42] R. Zallen, in *II-VI Semiconducting Compounds*, ed. D. G. Thomas, W. A. Benjamin, Inc., New York, 1967, pp. 877–887.

[43] G. Roberts and R. Zallen, *Journal of Physics C: Solid State Physics*, 1971, **4**, 1890.

[44] G. A. Soler, J.-P. Aicardi and J.-P. Leyris, *physica status solidi (b)*, 1981, **105**, 249–255.

[45] S. Deb, *Physical Review B*, 1970, **2**, 5003–5007.

[46] M. J. Weber, *Handbook of Optical Materials*, CRC Press, 2002, p. 536.

[47] G. Massé, J. P. Aicardi and J. P. Leyris, *Physica Status Solidi (a)*, 1977, **43**, 191–201.

[48] M. Cardona, R. Kremer, G. Siegle, A. Muñoz, A. Romero and M. Schmidt, *Physical Review B*, 2010, **82**, 085210.

[49] E. H. Carlson, *Journal of Crystal Growth*, 1967, **1**, 271–277.

[50] K. Paquette and G. Helz, in *Mercury as a Global Pollutant*, ed. D. B. Porcella, J. W. Huckabee and B. Wheatley, Springer Netherlands, Dordrecht, 1995, pp. 1053–1056.

[51] G. A. Parks and D. K. Nordstrom, in *Chemical Modeling in Aqueous Systems*, ed. E. A. Jenne, American Chemical Society, Washington, D. C., 1979, vol. 93, ch. 18, pp. 339–352.

[52] D. Rickard, *Reviews in Mineralogy and Geochemistry*, 2006, **61**, 421–504.

[53] A. Vogler and H. Kunkely, *Topics in Current Chemistry*, 2001, **213**, 143.

[54] H. Zhang, in *Recent Developments in Mercury Science*, ed. D. A. Atwood, Springer-Verlag, Berlin/Heidelberg, 2006, vol. 120, pp. 37–79.

[55] H. Kunkely and A. Vogler, *Chemical Physics Letters*, 1993, **206**, 467–469.

[56] H. Kitamura, *Chemical Physics*, 2006, **325**, 207–219.

[57] M. Kaupp and H. G. von Schnering, *Inorganic Chemistry*, 1994, **33**, 4179–4185.

[58] H. Kunkely, O. Horváth and A. Vogler, *Coordination Chemistry Reviews*, 1997, **159**, 85–93.

[59] J. Cheng and M. Sprik, *Physical Review B*, 2010, **82**, 081406.

[60] Y. Wu, M. K. Y. Chan and G. Ceder, *Physical Review B*, 2011, **83**, 235301.

[61] S. Lebègue, B. Arnaud, M. Alouani and P. Bloechl, *Physical Review B*, 2003, **67**, 155208.

[62] R. Godby and R. Needs, *Physical Review Letters*, 1989, **62**, 1169–1172.

[63] M. Hybertsen and S. Louie, *Physical Review B*, 1986, **34**, 5390–5413.

[64] D. Johnson, *Physical Review B*, 1974, **9**, 4475–4484.

[65] M. Stankovski, G. Antonius, D. Waroquiers, A. Miglio, H. Dixit, K. Sankaran, M. Giantomassi, X. Gonze, M. Côté and G.-M. Rignanese, *Physical Review B*, 2011, **84**, 241201.